Supporting Information

Interfacial Engineering of Polyphenylene Sulfide Fiber Membrane for High-Performance Alkaline Water Electrolysis

Tao Zhuang [a], Qixuan Zhu [a], Chao Chen [a, b, c], Jia Zhang [a], Yuxiang Xu [a, d], Yi Wang [a], Zhiqiang Lu [a, d], Weiwei Wang [a, d], Guiyin Xu [a, *]

[a] State Key Laboratory of Advanced Fiber Materials, College of Materials Science and Engineering, Donghua University, Shanghai 201620, China

[b] Henan Academy of Sciences, Zhengzhou 450001, China

[c] School of Materials Science and Engineering, Zhengzhou University, Zhengzhou 450001, China

[d] Ancan Technology LTD, Jiangsu 214400, China

[*] Corresponding Authors: xuguiyin@dhu.edu.cn

Supplementary Figures & Tables

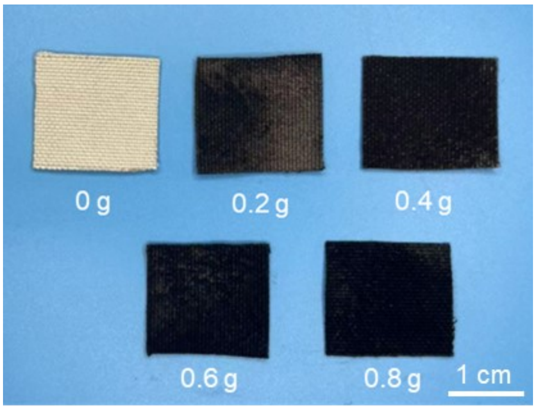

Fig. S1. Digital photos of the membranes with different-mass dopamine (0, 0.2, 0.4, 0.6 and 0.8 g). The surfaces darken from yellow to black as dopamine loading increases, forming a denser surface layer.

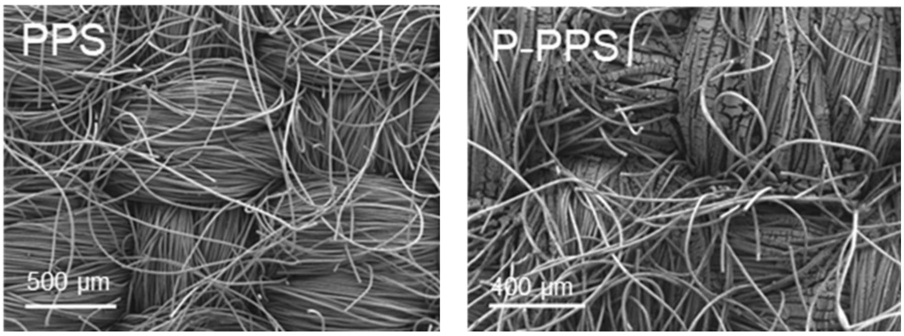

Fig. S2. Top-view surface SEM images of the PPS and P-PPS fiber membranes.

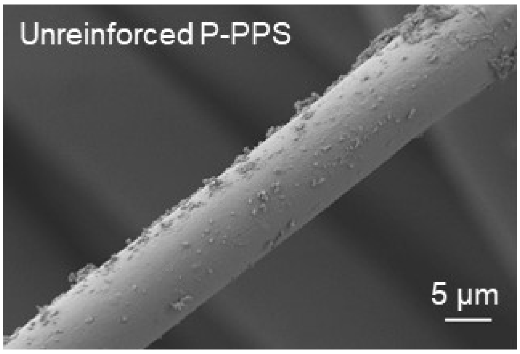

Fig. S3. Surface SEM image of the unreinforced P-PPS fiber membrane. The surface SEM image reveals uneven PDA distribution, with discontinuous patches present only in localized regions of the fiber surface.

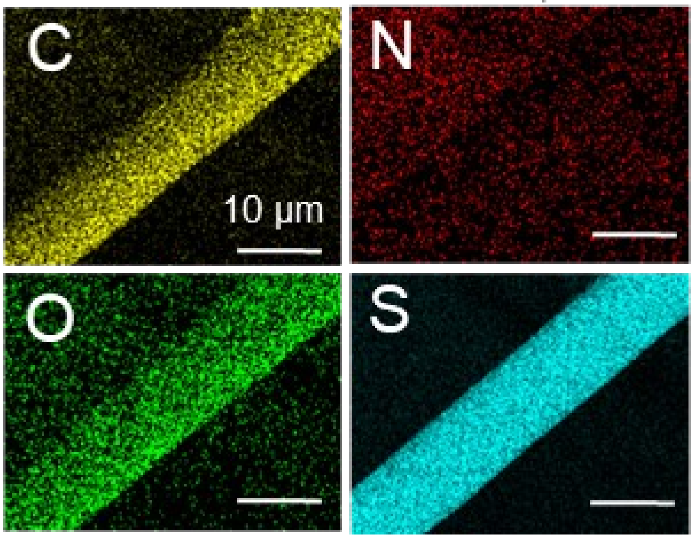

Fig. S4. EDS mapping of the PPS fiber membrane for elements C, N, O, S. The results indicate the presence of C and S as the primary components, along with minor O. No signal for N is detected.

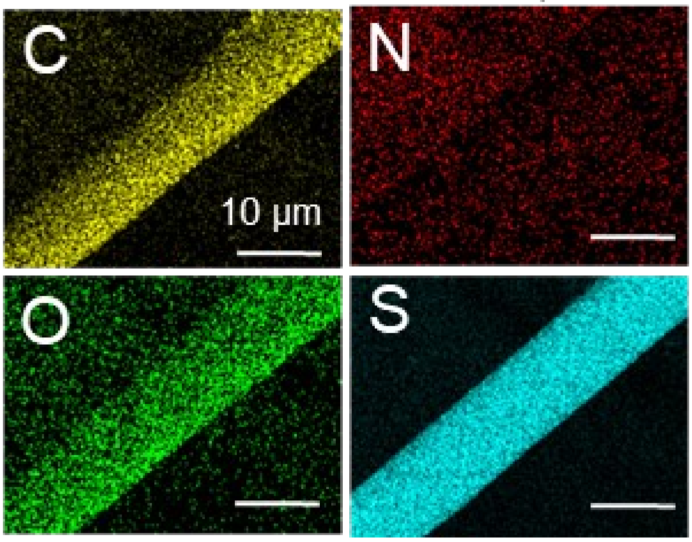

Fig. S5. EDS mapping of the unreinforced P-PPS fiber membrane. The results confirm the presence of C, O, and S as the major elements, while N is detected only in minor amounts.

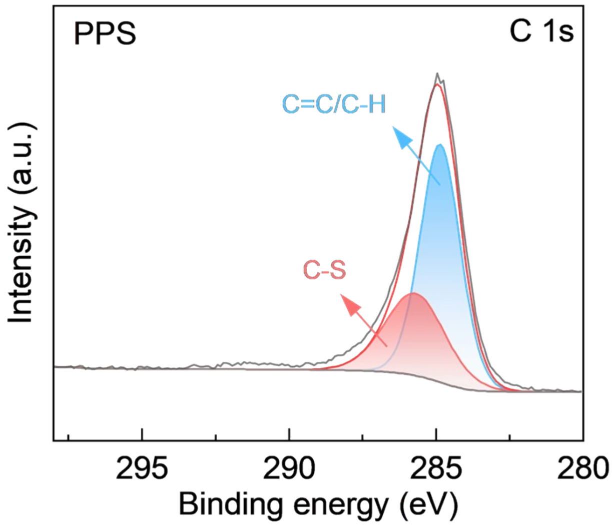

Fig. S6. C 1s XPS spectrum of the PPS fiber membrane.

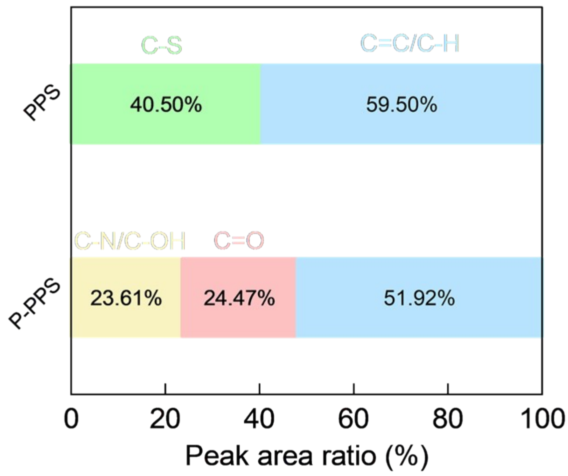

Fig. S7. The peak area ration of C 1s of the PPS and P-PPS fiber membranes. The C 1s peak area ratios reveal PPS contains mainly C-S and C=C/C-H bonds, while P-PPS features additional C-N/C-OH bonds from dopamine modification, confirming successfully PDA encapsulation.

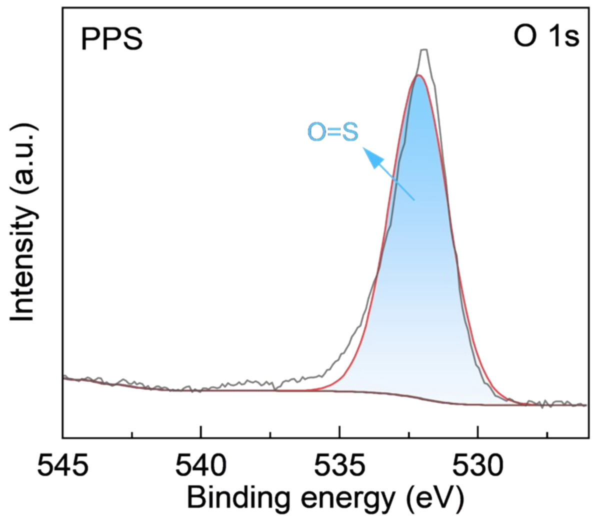

Fig. S8. O 1s XPS spectrum of the PPS fiber membrane.

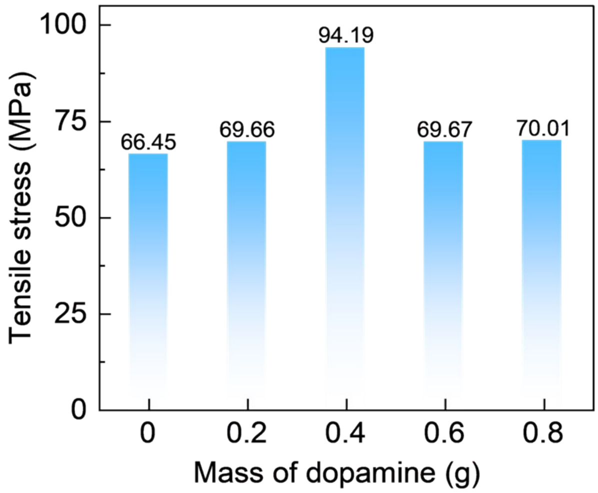

Fig. S9. Tensile strength of the membranes with different-mass dopamine. The tensile strength of the membranes is enhanced by dopamine addition, reaching the highest value at 0.4 g.

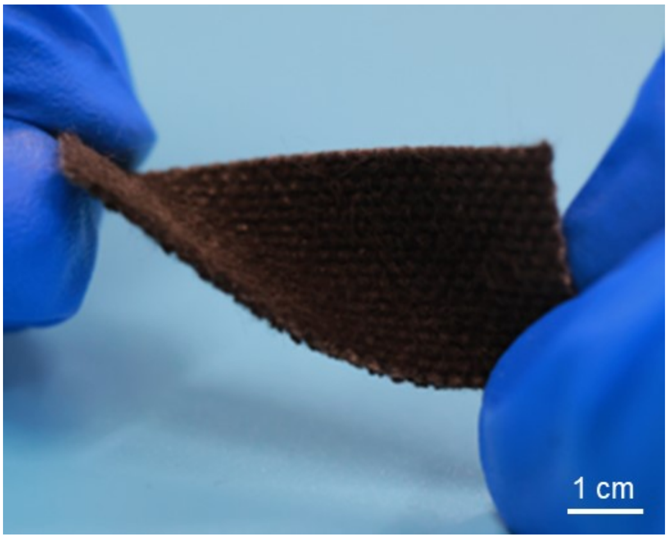

Fig. S10. Excellent flexibility of the P-PPS fiber membrane.

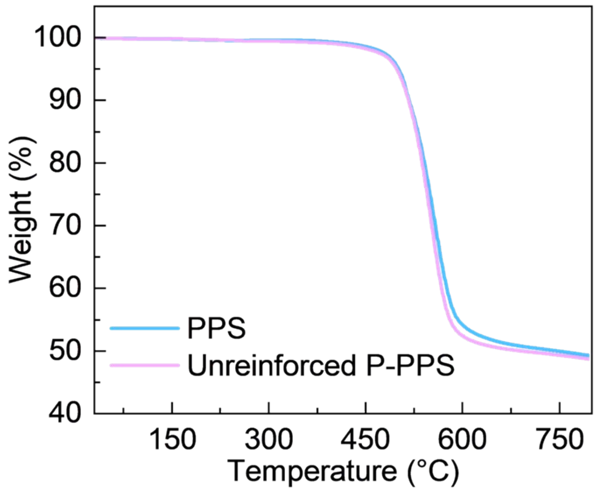

Fig. S11. TGA curves of the PPS and unreinforced P-PPS fiber membranes.

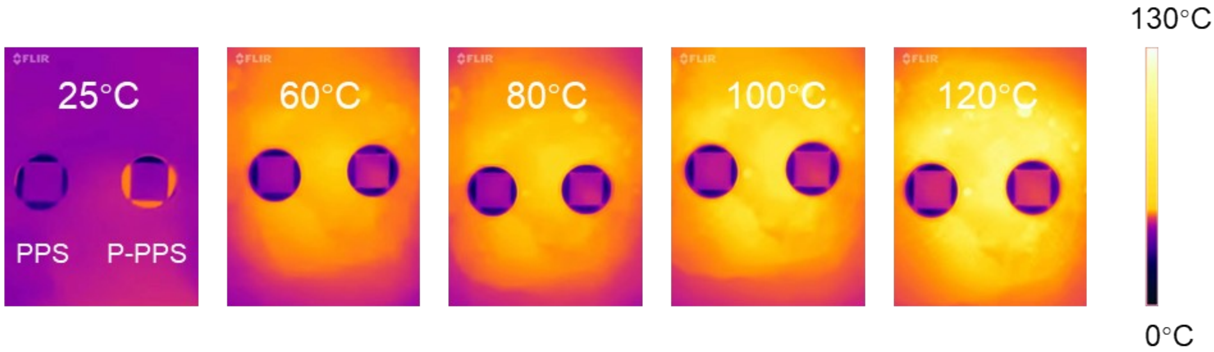

Fig. S12. Digital images of thermal shrinkage of the PPS and P-PPS fiber membranes after heat treatment at different temperatures for half an hour. The P-PPS fiber membrane maintains its structural integrity and exhibits no noticeable shrinkage even when subjected to high temperatures, demonstrating superior thermal stability.

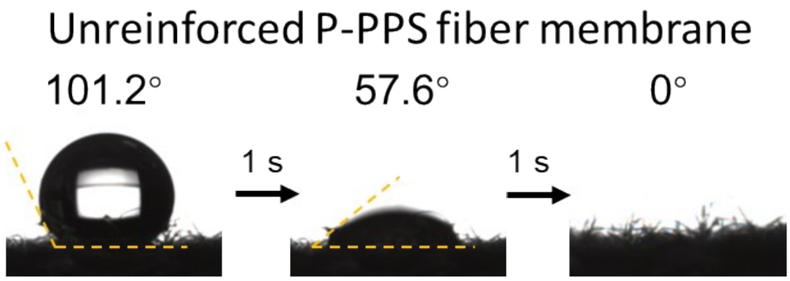

Fig. S13. Water contact angles of the unreinforced P-PPS fiber membrane. The rapid wetting behavior of the unreinforced P-PPS fiber membrane demonstrates its excellent hydrophilic properties.

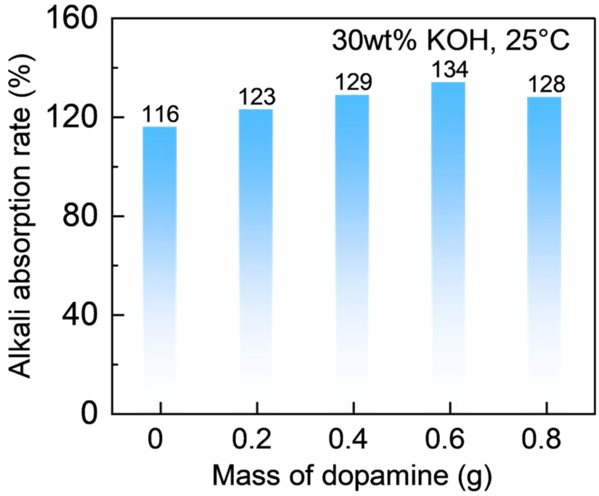

Fig. S14. Alkali absorption rate of the fiber membranes with different-mass dopamine.

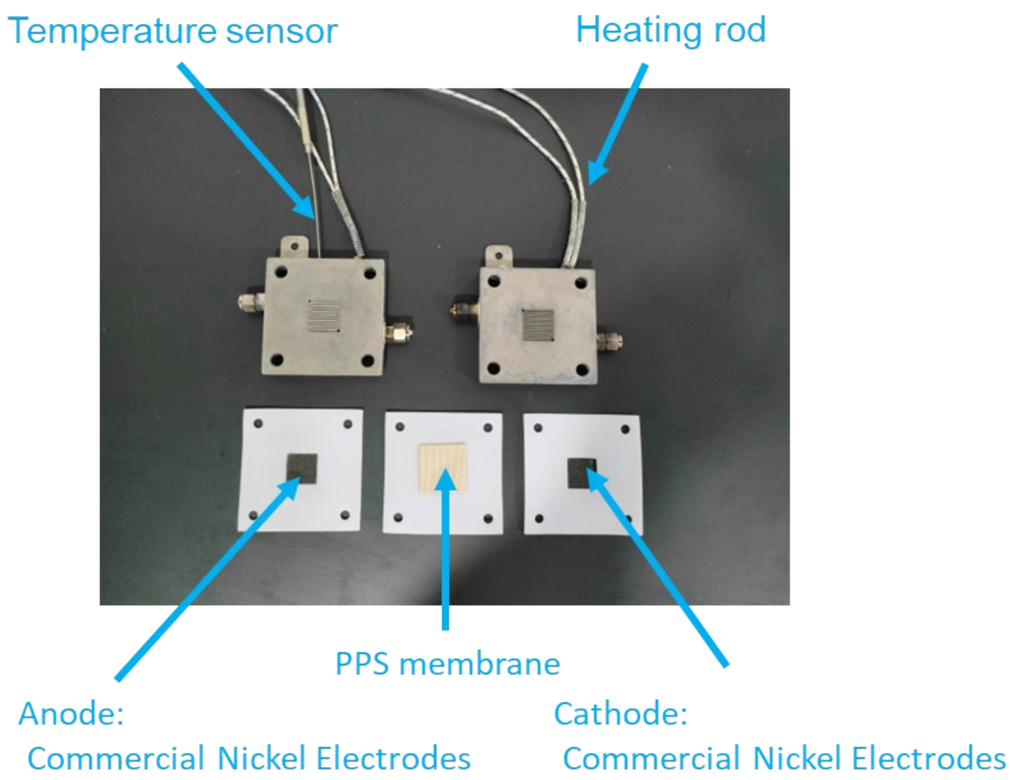

Fig. S15. Physical drawing of a zero-gap electrolyzer for testing membrane electrolysis performance and stability.

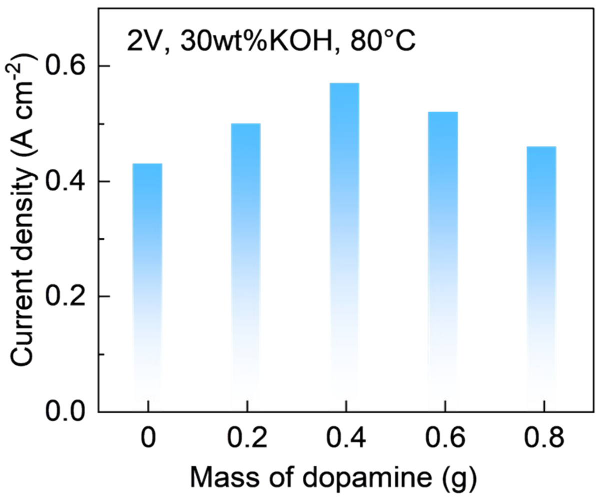

Fig. S16. Comparisons of the current density of membranes with different-mass dopamine at the voltage of 2 V.

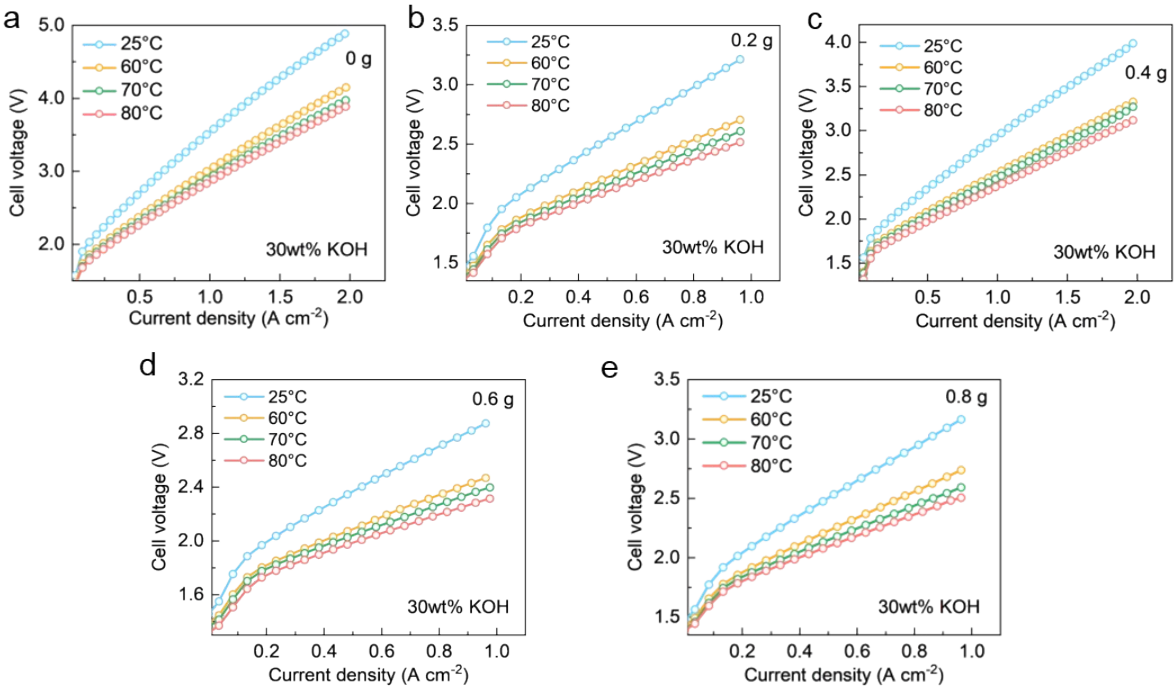

Fig. S17. Polarization curves of the membranes with different-mass dopamine in 30wt% KOH solution at different operating temperature.

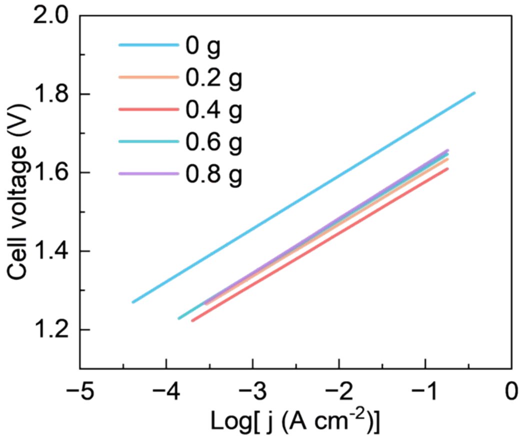

Fig. S18. Tafel slope of the membranes with different-mass dopamine at 80°C in 30wt% KOH.

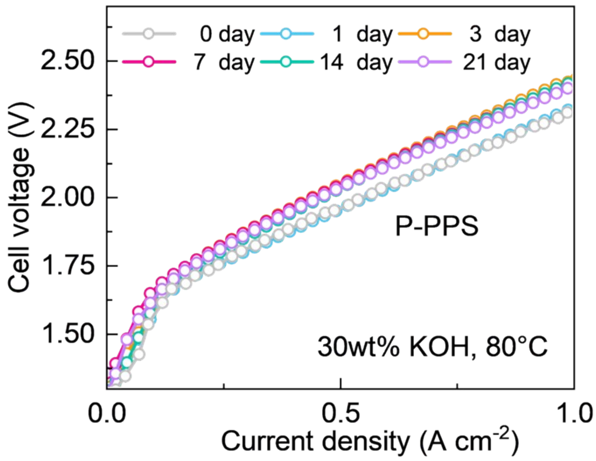

Fig. S19. Polarization curves of P-PPS fiber membrane in 30wt% KOH at 80°C for different durations.

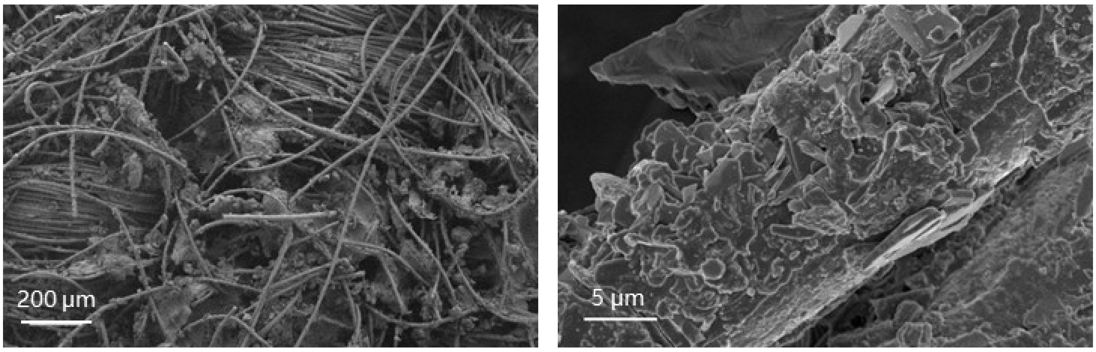

Fig. S20. Surface SEM images of the P-PPS fiber membrane after 14 days of immersion in 30wt% KOH solution at 80°C. The polydopamine remains stably adhered to the fiber membrane surface after 14 days of immersion, demonstrating its remarkable chemical stability.

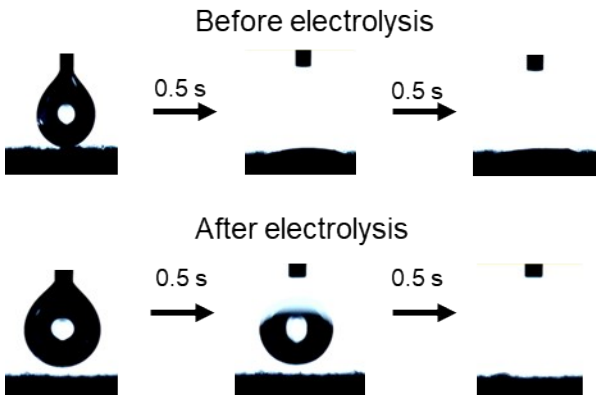

Fig. S21. Comparison of water contact angles of P-PPS fiber membrane before and after electrolysis.

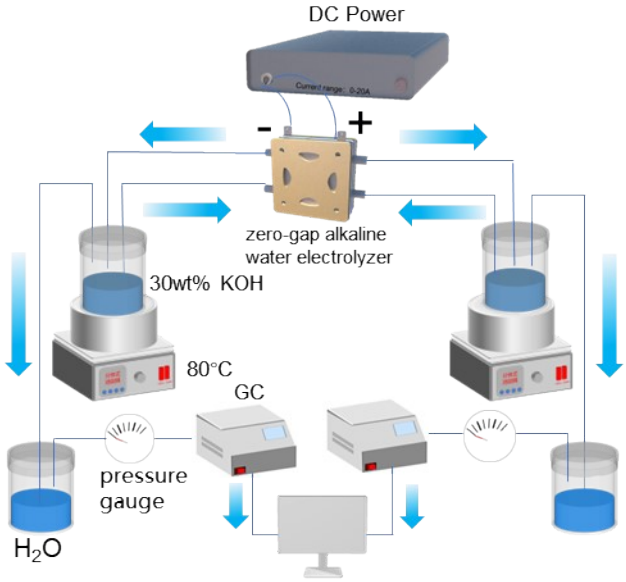

Fig. S22. Schematic diagram of the gas purity detection device.

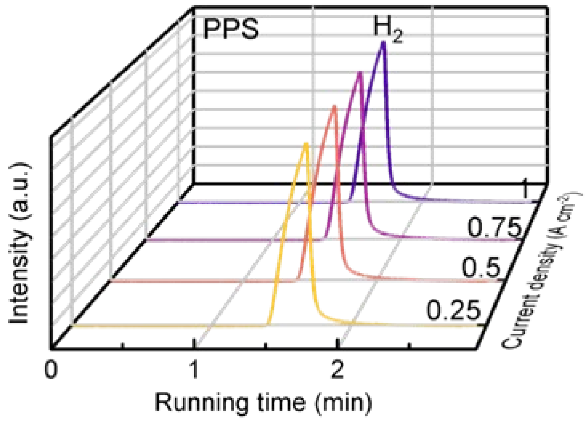

Fig. S23. H_2 purities at different current densities were measured using gas chromatograph, with online spectra recorded for PPS fiber membrane.

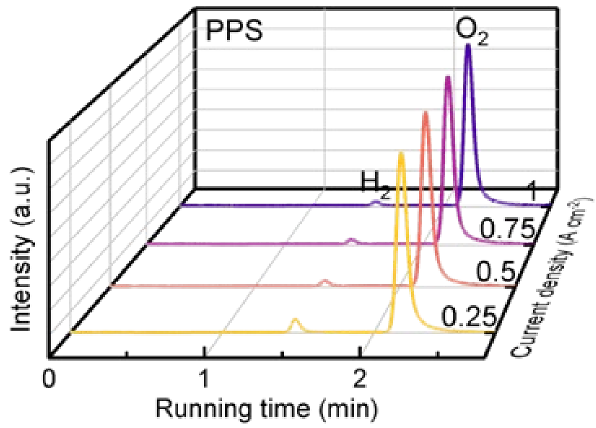

Fig. S24. O_2 purities at different current densities were measured using gas chromatograph, with online spectra recorded for PPS fiber membrane.

Table S1. Comparison of mechanical properties of prepared and commercial membranes.

Different-mass dopamine (g)	Tensile strength (MPa)	Elongation at break (%)
0	66.45±0.89	43.47±0.55
0.2	69.66±0.18	36.64±0.21
0.4	94.19±0.75	46.64±0.69
0.6	69.67±0.31	36.97±0.21
0.8	70.01±0.65	40.97±0.39

Table S2. Physical parameters of prepared and commercial membranes.

Different-mass dopamine (g)	Thickness （μm）	Porosity （%）	Average pore diameter （μm）	Largest pore diameter (μm)
0	850±50	47.30	4.12	18.02
0.2	900±10	37.99	5.77	33.90
0.4	950±30	30.86	4.51	25.01
0.6	970±20	26.88	5.34	31.78
0.8	990±10	30.27	5.59	30.92

Table S3. Tafel slope variations with different-mass dopamine.

Different-mass dopamine (g)	Tafel Slope ($mV\ dec^{-1}$)
0	130
0.2	132
0.4	130
0.6	129
0.8	133

Table S4. Electrochemical impedance of the membranes.

Different-mass dopamine (g)	R1 (Ω cm^2)	R2 (Ω cm^2)	R3 (Ω cm^2)	CPE1-T (S s^n cm^{-2})	CPE1-P (S s^n cm^{-2})	CPE2-T (S s^n cm^{-2})	CPE2-P (S s^n cm^{-2})
0	0.057	0.061	0.269	0.909	0.911	1.213	0.725
0.2	0.056	0.088	0.191	9.003×10^{-4}	0.792	1.128	0.723
0.4	0.054	0.065	0.216	3.927×10^{-4}	0.887	1.951	0.617
0.6	0.061	0.061	0.298	1.568×10^{-4}	0.970	2.349	0.526
0.8	0.063	0.062	0.421	1.708×10^{-4}	0.967	2.876	0.452

Table S5. Comparion of electrochemical performance of different membranes reported in previous literature.

Membrane	Anode	Cathode	Temperature (°C)	Electrolyte (wt%)	Current density (A cm^{-2})	Durability (h)	Reference
P-PPS	Nickel-based electrodes	Nickel-based electrodes	80	30wt% KOH	0.6 A cm^{-2} @ 2.03 V	200	This work
N-T-PPS	Ni-Fe	Ni-Mo	80	30wt% KOH	0.493 A cm^{-2} @ 2 V	500	[1]
SHL-PPS	Ni foam	Ni-Mo foam	80	30wt% KOH	0.5 A cm^{-2} @ 1.90 V	120	[2]
DEA-ZrO_2	Ni foam	Ni foam	80	30wt% KOH	0.485 A cm^{-2} @ 2 V	150	[3]
Z60	Ni foam	Ni foam	80	6 M KOH	0.5 A cm^{-2} @ 2 V	400	[4]
$Z_{77}LDH_8$/PSU	Ni foam	Ni foam	80	30wt% KOH	0.59 A cm^{-2} @ 2 V	150	[5]
PcPBI-Im-C	Ni	Ni	80	1 M KOH	0.454 A cm^{-2} @ 2.10 V	100	[6]
cPBI-0.4p-0.6s	IrO_2	Pt/C	80	1 M KOH	0.553 A cm^{-2} @ 2.10 V	10	[7]
PcPBI-Nb-C2	IrO_2	Pt/C	60	1 M KOH	0.368 A cm^{-2} @ 2.10 V	8.3	[8]
PBI/mTPN	Ni-Fe	Ni-Mo	50	1 M KOH	0.250 A cm^{-2} @ 1.98 V	200	[9]
CS-G-PAENA-50	IrO_2	Pt/C	60	1 M KOH	0.490 A cm^{-2} @ 2.50 V	66	[10]
ABPBI-c-PVBC/OH (1:2)	IrO_2	Pt/C	50	1 M KOH	0.380 A cm^{-2} @ 1.98 V	/	[11]

References

[1] Y. Tang, W. Song, M. Guo, G. Yang, K. Su, M. Zhang, Z. Li, Hydrophilic modified polyphenylene sulfide fabric separator for efficient alkaline water electrolysis, Int. J. Hydrogen Energy 126 (2025) 66-76. https://doi.org/10.1016/j.ijhydene.2025.03.401.

[2] Y. Wang, X. Huo, M. Peng, M. Zhang, X. Liu, J. Zhang, W. Li, Superhydrophilic polyphenylene sulfide membrane with enhanced ion transfer for alkaline water electrolysis, Int. J. Hydrogen Energy 65 (2024) 872-880. https://doi.org/10.1016/j.ijhydene.2024.04.006.

[3] X. Yuan, T. Yan, Z. Liu, P. Kang, Highly efficient alkaline water electrolysis using alkanolamine-functionalized zirconia-blended separators, ACS Sustainable Chem. Eng. 11(10) (2023) 4269-4278. https://doi.org/10.1021/acssuschemeng.2c07618.

[4] H. Li, X. Hu, K. Geng, M. Liu, B. Hu, Q. Chen, Z. Jiang, M. He, Y. Huang, N. Li, Z. Xu, Q. Zhang, Highly hydrophilic polybenzimidazole/zirconia composite separator with reduced gas crossover for alkaline water electrolysis, J. Membr. Sci. 683 (2023) 121844. https://doi.org/10.1016/j.memsci.2023.121844.

[5] Z. Meng, Z. Liu, P. Kang, LDH-blended ZrO_2/polysulfone composite membrane for alkaline water electrolysis, ACS Sustainable Chem. Eng. 13(21) (2025) 7717-7727. https://doi.org/10.1021/acssuschemeng.5c00182.

[6] M. Guo, Z. Wang, Y. Xu, X. Zhu, Vinyl-based in-situ crosslinked polybenzimidazoles for anion exchange membranes water electrolysis, J. Membr. Sci. 707 (2024) 123026. https://doi.org/10.1016/j.memsci.2024.123026.

[7] M. Guo, T. Ban, Y. Wang, X. Wang, Z. Wang, X. Zhu, Polybenzimidazoles incorporating imidazole N-spirocyclic quaternary ammonium cation for anion exchange membranes water electrolysis, J. Membr. Sci. 684 (2023) 121903. https://doi.org/10.1016/j.memsci.2023.121903.

[8] M. Guo, T. Ban, Y. Wang, X. Wang, X. Zhu, "Thiol-ene" crosslinked polybenzimidazoles anion exchange membrane with enhanced performance and durability, J. Colloid Interface Sci. 638 (2023) 349-362. https://doi.org/10.1016/j.jcis.2023.01.137.

[9] M. Najibah, E. Tsoy, H. Khalid, Y. Chen, Q. Li, C. Bae, J. Hnát, M. Plevová, K. Bouzek, J.H. Jang, H.S. Park, D. Henkensmeier, PBI nanofiber mat-reinforced anion exchange membranes with covalently linked interfaces for use in water electrolysers, J. Membr. Sci. 640 (2021) 119832. https://doi.org/10.1016/j.memsci.2021.119832.

[10] F. Zhu, Y. Zhan, J. Tang, X. Chen, S. Li, X. Lei, Construction of cross-linked poly(aryl ether nitrile) anion exchange membranes containing bilateral linked branches for water electrolyzer, ACS Appl. Polym. Mater. 6(14) (2024) 8377-8388. https://doi.org/10.1021/acsapm.4c01218.

[11] R.E. Coppola, D. Herranz, R. Escudero-Cid, N. Ming, N.B. D'Accorso, P. Ocón, G.C. Abuin, Polybenzimidazole-crosslinked-poly(vinyl benzyl chloride) as anion exchange membrane for alkaline electrolyzers, Renew. Energ. 157 (2020) 71-82. https://doi.org/10.1016/j.renene.2020.04.140.